THz SPICE for Modeling Detectors and Nonquadratic Response at Large Input Signal

Alexey Gutin, Trond Ytterdal, Valentin Kachorovskii, Andrey Muraviev, and Michael Shur, *Life Fellow, IEEE*

***Abstract*— The THz SPICE model is capable of simulating field effect transistors (FETs) in a plasmonic mode of operation at frequencies far above the device cutoff frequency. The model uses a distributed RC or RLC network and is validated by comparison of the simulation results with our analytical model of the plasmonic detector, and with measured results. It also allows us to determine the operation regimes, where conventional SPICE models are still applicable. The applicability of this model for THz sensing applications is demonstrated by simulating the plasmonic THz FET sensor with on-chip amplifier.**

***Index Terms*— Plasmonic detector, SPICE, sub-millimeter wave, terahertz detectors.**

I. Introduction

TRANSISTOR scaling has allowed circuit designers to push circuits to run at sub-THz frequencies [1]–[3]. Plasmonic Field Effect Transistors (FETs) have also been shown to work as detectors [4]–[7] and emitters [8]–[10] of terahertz radiation with higher responsivity and lower noise than commercially available products. Terahertz technology has potential for many sensing applications in security applications [11], [12], biomedical imaging [13], [14], and communications [15]. A major advantage of plasmonic FET technology for sensing applications is an ability to integrate sensing elements with on-chip amplifiers and readout and image processing circuitry. To enable such integration, we need compact CAD modeling tools to simulate plasmonic FET operation in a complex circuit environment.

Traditionally, digital circuits have been modeled using SPICE circuit simulators. However, the compact models used by SPICE fail to accurately model device physics, which become important as feature sizes decrease, operating frequencies increase, and when devices are modeled as a detector for terahertz radiation. The traditional SPICE models fail to accurately model the device operated in the plasmonic mode, when operating frequencies are much higher than f_T and $f_{\max}$. This paper describes a new THz SPICE model verified up to 2 THz, which addresses these issues, and can be used with any other compact modeling platform such as ADS [16] or CADENCE [17]. This is achieved by modeling the channel of a FET as a distributed RC or RLC network with distributed gate resistance, where traditional SPICE models these as lumped elements.

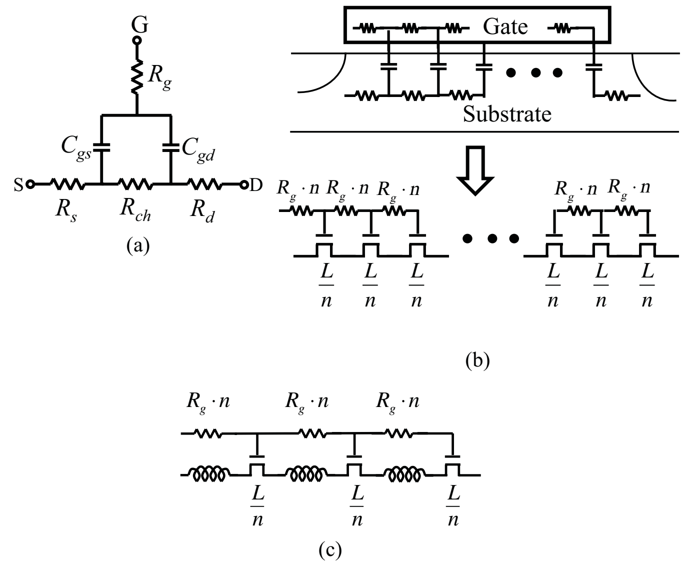

Fig. 1. (a) Traditional circuit representation of a FET in SPICE. (b) THz SPICE model split into n sections of gate length L/n (where L is gate length of the entire channel) with distributed RC representation of device channel and distributed gate resistance of R_g/n, along with equivalent SPICE model. (c) Model with inductive elements to account for electron kinetic inductance.

The model is validated using plasmonic detector measurements and our recent theory [18] that has explored nonquadratic response with respect to input signal at large intensities.

II. THz SPICE Model

The analytical [4]–[8] and computer [19], [20] models that have been developed to describe the response of a terahertz detector to radiation at low intensities do not account for device parasitics, bonding wires, and dependence on device width. Furthermore, these models are not suitable for simulating various circuit configurations or detector arrays. SPICE circuit simulators are a natural solution to these challenges, and provide a fast and accurate way to model and optimize terahertz detectors prior to fabrication.

Manuscript received June 14, 2012; revised September 19, 2012; accepted October 1, 2012. Date of publication October 11, 2012; date of current version December 6, 2012. This work was supported in part by the U.S. NSF under the auspices of I/UCRC "CONNECTION ONE," NSF I-Corp, the NSF EAGER Program, and in part by SRC and the Texas Analog Center of Excellence (TxACE) under task number 1836.079. The associate editor coordinating the review of this paper and approving it for publication was Dr. Francis P. Hindle.

A. Gutin, A. Muraviev, and M. Shur are with Rensselaer Polytechnic Institute, Troy, NY 12180 USA (e-mail: gutina2@rpi.edu; amuravie@gmail.com; shurm@rpi.edu).

T. Ytterdal is with the Norwegian University of Science and Technology, Trondheim 7034, Norway (e-mail: ytterdal@iet.ntnu.no).

V. Kachorovskii is with Ioffe Physical-Technical Institute, St. Petersburg 194021, Russia (e-mail: kachor.valentin@gmail.com).

Color versions of one or more of the figures in this paper are available online at http://ieeexplore.ieee.org.

Digital Object Identifier 10.1109/JSEN.2012.2224105

1530–437X/$31.00 © 2012 IEEE

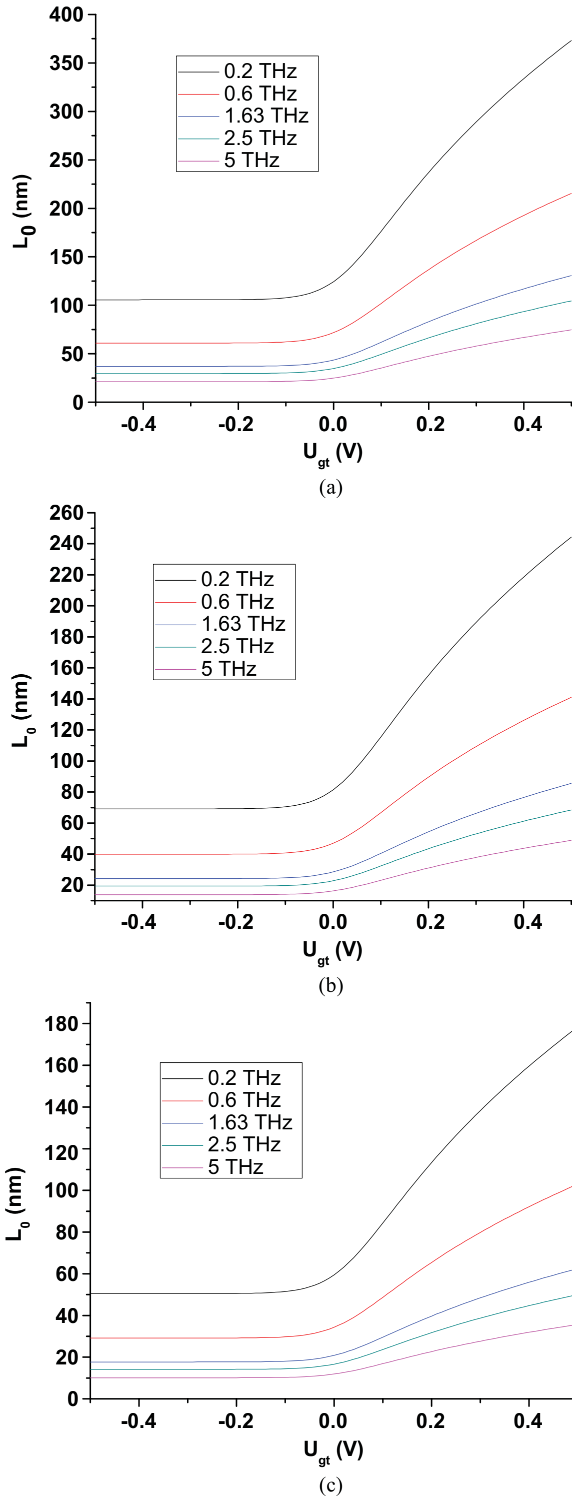

Fig. 2. Calculated characteristic length, L_0, as a function of gate swing voltage at different frequencies for (a) GaAs, (b) GaN, and (c) Si. The parameters used were the same as in Fig. 3.

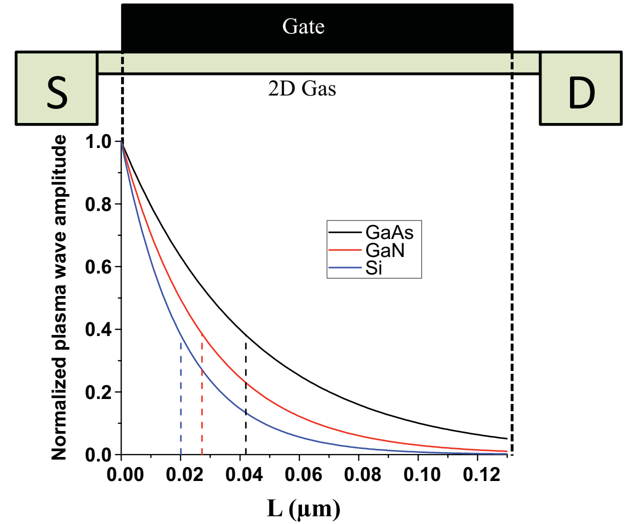

Fig. 3. Space dependence of electron oscillations excited by 1.63-THz signal at $U_{gt} = 0$ for GaAs (mobility of 3500 cm^2/Vs, effective mass of 0.067), GaN (mobility of 1500 cm^2/Vs, effective mass of 0.23), Si (mobility of 800 cm^2/Vs, effective mass of 0.19). Subthreshold ideality factor of 1.55 was used for all materials. Dashed lines represent characteristic length of decay, L_0, for each material.

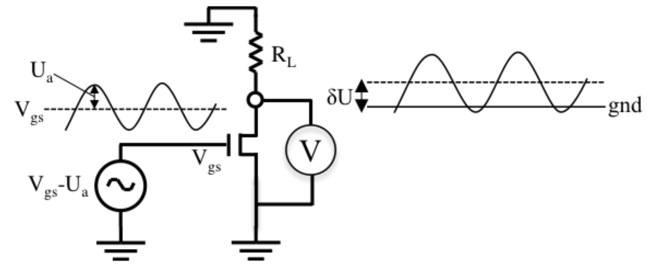

Fig. 4. Schematic of simulation circuit in open drain mode.

The channel and gate resistance of a FET in traditional SPICE is represented by lumped elements as seen in Fig. 1(a). This representation fails to accurately capture device physics of a plasmonic FET. Previous distributive resistive mixing models have been introduced [21] to describe the channel of a FET, but are valid for only nonresonant detectors, and did not have distributed gate resistance, which is important to model at high frequencies. At THz frequencies, the oscillations of the electron density excited in the FET channel–called plasma waves–might propagate and decay within a fraction of the device channel [22]–[24]. According to [25], the characteristic distance of the plasma wave decay (shown in Fig. 3) is given by

$$L_0 = \sqrt{\frac{\mu\, n}{\omega(dn/dU)\,|_{U=U_g}}} \tag{1}$$

where (see Ref [26])

$$n(U) = \frac{C\eta k_B T}{e^2}\ln\left[1+\exp\left(\frac{eU}{\eta k_B T}\right)\right] \tag{2}$$

and C is the gate-to-channel capacitance per unit area, η is the subthreshold ideality favor, k_B is the Boltzmann constant, T is temperature, e is the electronic charge, and U is the gate-to-channel voltage swing.

At high frequencies, $L_0 < \mathrm{L}$, the single channel lumped element model becomes inaccurate, especially close to and below the threshold, where dn/dU is small (see Fig. 2).

To capture these device physics we use the distributive model for the channel capacitance and resistance and the gate

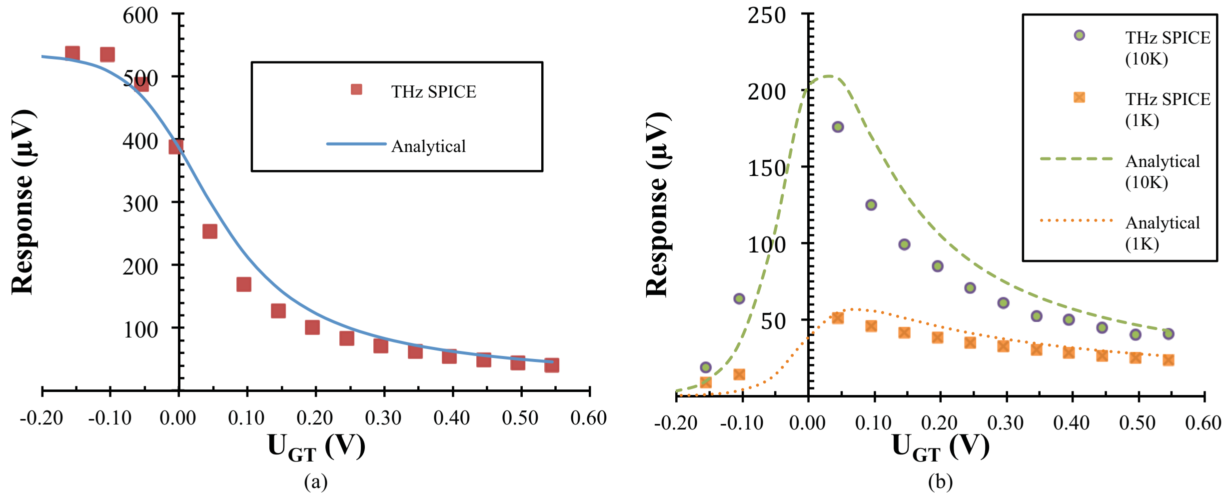

Fig. 5. (a) Comparison between the analytical model from [26] and THz SPICE model in open drain mode. b) Analytical model and THz SPICE model at several load resistances.

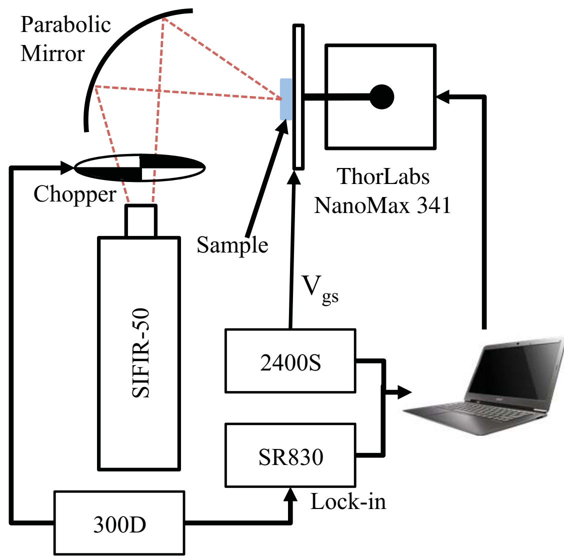

Fig. 6. Experimental setup used for measurements at 1.63 THz.

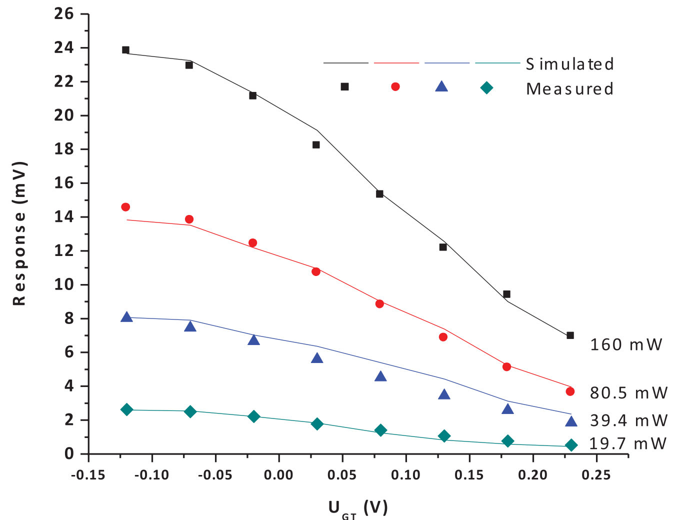

Fig. 7. Comparison between THz SPICE simulation and measured data of varying output power levels at 1.63 THz.

resistance as shown in Fig. 3(b), with each section being smaller than L_0. All simulations in this work used a model of four sections.

The model shown in Fig. 3(b) does not account for the electron inertia, and, therefore, is only applicable to the nonresonant regime of operation (decaying plasma waves). However, this model could be generalized by inclusion of the inductive elements [as shown in Fig. 3(c)], such that the resonance frequency of this distributive circuit equals the plasma wave frequency for the appropriate boundary conditions. Such model and its implications will be considered elsewhere.

For each section, we use the following model equations (see Table I for brief summary of parameters and Appendix for detailed list of parameters and typical values). In the sub-threshold region, the drain-to-source current I_{ds} is given by:

$$I_{ds} = I_{dson}.\exp\left(\frac{V_{gs}-V_{on}}{X_n V_{th}}\right)$$
$$X_n = 1+\frac{q.N_{fs}}{c_{ox}}+\frac{1}{2}\left(\frac{\gamma.\lambda_s}{\sqrt{\varphi - V_{bs}}}+\lambda_n\right). \quad (3)$$

Above threshold, I_{ds} is given by:

$$I_{ds} = I_{ds_at} = \beta\left(V_{gs}-V_T-\frac{1+\lambda_b}{2}V_{dsm}\right)V_{dsm}$$
$$\beta = U_{eff}c_{ox}\frac{W_{eff}}{L_{eff}}. \quad (4)$$

III. Model Validation

A generalized expression to characterize device response at large and small signals above and below the threshold voltage

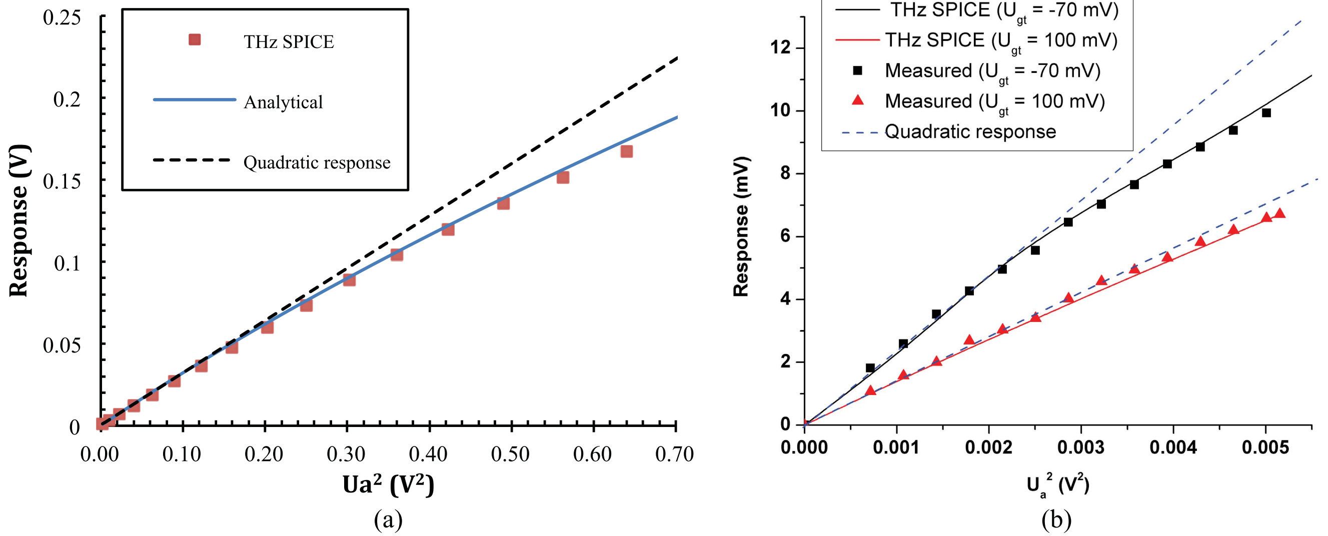

Fig. 8. (a) Comparison of the analytical model from (5), THz SPICE simulation, and the response of a quadratic detector. (b) Comparison of THz SPICE simulation and measured data above threshold ($U_{gt} = -70$ mV) and below threshold ($U_{gt} = 100$ mV).

can be expressed as

$$\delta U = \frac{\eta K_B T}{c} \text{In} I_0 \left(\frac{eU_a}{\eta K_B T} \right) \tag{5}$$

where I_0 is the Bessel function of the imaginary argument, and U_a is the voltage coupled at the gate. Above threshold, device response at large intensities can be expressed as

$$\delta U = \frac{U_a^2}{2\left(\sqrt{U_{gt}^2 + U_a^2/2} + U_{gt}\right)} \tag{6}$$

Detectors can operate in photoconductive or photovoltaic regimes. In the photoconductive regime, drain current is used to bias the detector and increase response at the expense of higher flicker noise. In the photovoltaic mode, the drain of the detector is left floating, limiting noise only to thermal.

This paper studies the detector operated in the photovoltaic regime. Fig. 4 shows the equivalent circuit simulated using the distributed THz SPICE model. A sinusoidal wave of amplitude U_a representing the THz field coupled to the device is superimposed on a DC bias, V_{gs}, at the gate. In the absence of THz radiation, the voltage at the drain is zero. Once radiation is applied, a sinusoidal wave is seen at the drain. Integrating this wave over time establishes a DC shift representing the THz response of the detector, δU.

The analytical model open drain response was obtained using the same gate length, subthreshold ideality factor, and temperature as were used for the THz SPICE model. Fig. 5(a) shows the THz response as a function of applied gate-bias voltages. As seen, there is a strong agreement between the analytical and THz SPICE models. Adding a load resistor of finite value creates a voltage divider circuit between the channel resistance and load [27], and significantly affects the measured response. Fig. 5(b) shows the detector response as a function of gate-bias voltage at finite loads for both the analytical (Eq. 23 in Ref. 26) and THz SPICE models.

TABLE I
SPICE Model Parameters

Name	Parameter	Typical value
V_{gs}	Gate-to-source voltage	-
V_{ds}	Drain-to-source voltage	-
V_{dsat}	Drain saturation voltage	-
V_{dsm}	Minimum voltage between V_{ds} and V_{dsat}	-
V_{bs}	Bulk-to-source voltage	0 V
V_T	Threshold voltage	−0.18 V
V_{on}	Modified threshold voltage	-
γ	Bulk threshold parameter	0.43 $V^{1/2}$
λ_s	Effect of the short channel	-
λ_n	Specifies narrow width effect	-
λ_b	Effect of small geometry on saturation voltage	-
c_{ox}	Oxide capacitance per unit area	0.56 $\mu F/cm^2$
φ	Surface potential	0.8 V
N_{fs}	Surface state density	10^{12} $1/cm^2$
U_{eff}	Effective surface mobility	3500 cm^2/Vs
W_{eff}	Effective width	10 μm
L_{eff}	Effective length	0.13 μm

Capacitive loading effects [28] were estimated to be negligible and ignored.

To compare the THz SPICE model to measured results, we used a 0.13 μm × 10 μm depletion-mode InGaAs/GaAs HEMT from TriQuint Semiconductor. Fig. 6 shows a schematic of the experimental setup. An optically pumped THz gas laser (Coherent SIFIR-50) operating at 1.63 THz was used for terahertz radiation. The laser features a built-in output power monitor, which was used for output power

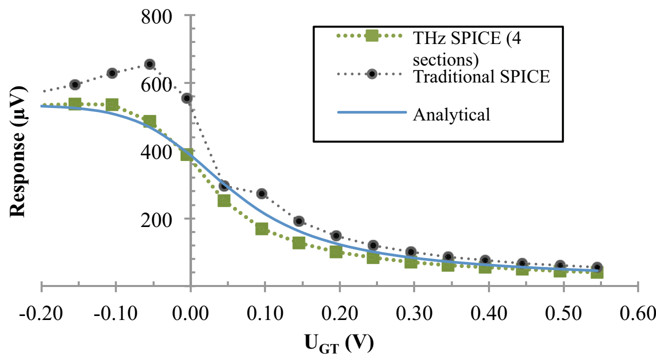

Fig. 9. Comparison of traditional SPICE model with lumped elements, THz SPICE model using distributed elements, and the analytical model from [26].

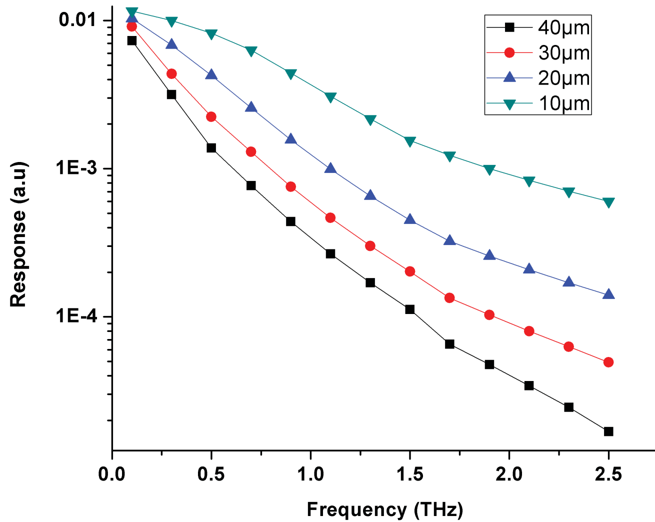

Fig. 10. Simulated response as a function of frequency at different device widths.

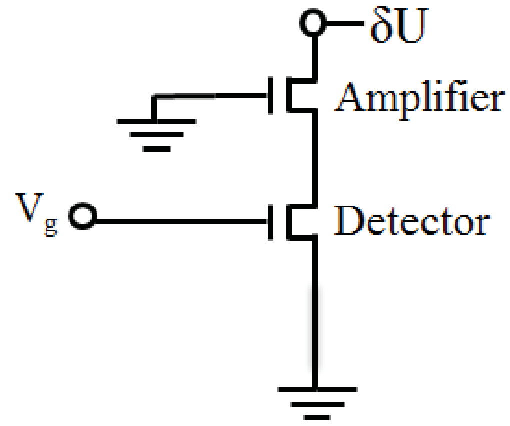

Fig. 11. Circuit schematic of detector and amplifier circuit.

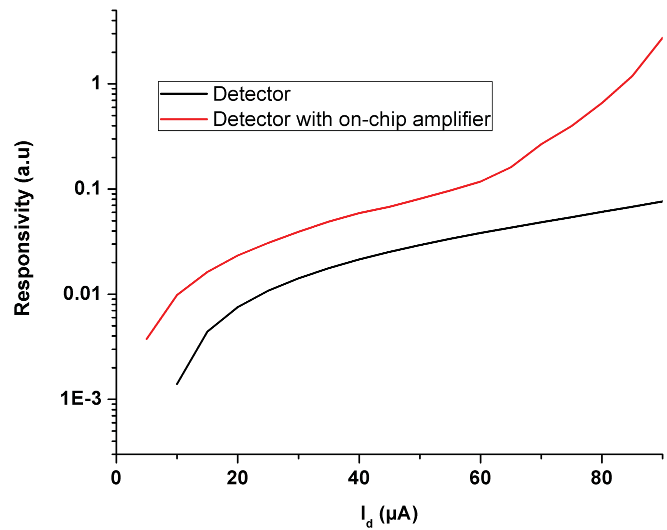

Fig. 12. Simulated comparison of detector with and without on-chip amplifier circuit.

calibration. The beam was modulated using an optical chopper operating at 210 Hz, and was focused on the sample using a parabolic mirror such that electric field polarization was in the direction of current in the device. The detector was mounted on a computer controlled three-axis nano-positioning stage (ThorLabs NanoMax 341), which was used to find maximum response and focus. A lock-in amplifier (Scientific Instruments SR-830) was used to measure the response, δU.

The laser was operated at varying power levels, and detector response was measured as a function of gate voltage. A THz SPICE model matched to the parameters extracted from the device was used to simulate response at different values of U_a corresponding to the output power levels of the laser. Fig. 7 shows close agreement between measured data and corresponding THz SPICE simulation results.

The analytical model developed in Eqs. 5 and 6 was also simulated using the THz SPICE model and compared to a quadratic detector response. Fig. 8(a) shows close agreement between simulated response using THz SPICE and the analytical model. There is also a clear divergence at large amplitude signals, representing high output intensity. Detector response was also measured as a function of the laser output power. Fig. 8(b) shows simulated nonquadratic response at high intensities, and close agreement with measured results.

Fig. 9 shows terahertz response as a function of gate-bias voltage for the analytical, traditional SPICE, and THz SPICE models of distributed in various sections. It can be clearly seen that the traditional SPICE model deviates substantially from analytical theory, especially below threshold. Since maximum terahertz response is observed subthreshold, it is critical to have a model accurate below and above threshold. The THz SPICE models distributed between four sections show close agreement with the analytical model.

It has been experimentally shown that response to terahertz radiation degrades with increasing frequency [29]. As a result, the effect of parasitics on device response is important to model. SPICE is uniquely suitable to model the dependence of parasitics on terahertz response. Fig. 10 shows the dependence of terahertz response as a function of incident frequency at several gate widths. It can be seen that terahertz response drops with higher frequency at larger gate widths, which is consistent with experimental data.

IV. Circuit Simulation Example

THz sensing applications require high sensitivity and low noise. This can be achieved by using on-chip amplification using a circuit shown in Fig. 11 [30].

Fig. 12 compares the simulated responsivity with and without the on-chip amplifications obtained using the THz SPICE. This example clearly illustrates the model capability.

V. Conclusion

In summary, we have developed a new THz SPICE model capable of accurately simulating FETs at terahertz frequencies. This model characterizes the device channel as a distributed RC or RLC network, compared to traditional SPICE models which characterize the channel by lumped elements. We have shown close agreement between THz SPICE, analytical model, and measured results. The THz SPICE model can be used in any compact modeling platform, and can be used to simulate and optimize terahertz detectors prior to fabrication. This model also paves the way for more accurate simulations for digital circuit designers as circuits move closer to operating at terahertz frequencies.

Appendix

Berkeley SPICE Level 3 Model Equations

In the sub-threshold region, the drain-source current I_{ds} is zero if the model parameter N_{fs} is not specified. Otherwise, I_{ds} is given by

$$I_{ds} = I_{dson}.\exp\left(\frac{V_{gs} - V_{on}}{X_n V_{th}}\right)$$

where V_{th} is the thermal voltage.

Above threshold Ids is given by

$$I_{ds} = I_{ds_at} = \beta\left(V_{gs} - V_T - \frac{1+\lambda_b}{2}V_{dsm}\right)V_{dsm}.$$

Definitions of the different quantities are given below.

$$\beta = U_{eff} c_{ox}\frac{W_{eff}}{L_{eff}}$$

$$c_{ox} = \frac{\varepsilon_{si}}{t_{ox}}$$

$$\lambda_b = \lambda_n + \frac{\gamma\,\lambda_S}{4\sqrt{\phi - V_{bs}}}$$

$$I_{dson} = I_{ds_at}\left(V_{on}, V_{dsm}, V_{bs}\right)$$

$$V_{dsm} = \min\left(V_{ds}, V_{dsat}\right)$$

If $V_{\max} \leq 0$

$$V_{dsat} = V_{sat}$$

else

$$V_{dsat} = V_{sat} + V_c - \sqrt{V_{sat}^2 + V_c^2}$$

$$V_{sat} = \frac{V_{gs} - V_T}{1+\lambda_b}$$

$$V_{on} = V_T + V_{th}.X_n$$

$$X_n = 1 + \frac{q.N_{fs}}{c_{ox}} + \frac{1}{2}\left(\frac{\gamma.\lambda_s}{\sqrt{\phi - V_{bs}}} + \lambda_n\right)$$

TABLE II

Parameter List and Typical Values

Name	Parameter	Units	Typical value
V_{T0}	Zero-bias threshold voltage	V	-0.18
γ	Bulk threshold parameter	$\sqrt{V}$	0.43
φ	Surface potential	V	0.6
ε_{si}	Dielectric constant of Silicon	F/m	1.0359×10^{-10}
t_{ox}	Gate oxide thickness	m	10^{-7}
N_{sub}	Substrate doping	1/cm^3	10^{17}
N_{fs}	Surface state density	1/cm^2	10^{12}
X_j	Metallurgical junction depth	m	3×10^{-9}
L_d	Lateral diffusion	m	31×10^{-12}
U_0	Surface mobility	cm$^2/V_s$	3500
$V_{\max}$	Maximum drift velocity for carriers	m/s	8288
δ	Width effect on threshold voltage	-	0.0
θ	Mobility modulation	1/V	0.0
η	Static feedback	-	0.0
κ	Saturation field factor	-	0.2
L	Drawn gate length	m	0.13 μm
W	Drawn gate width	m	10 μm

$$V_T = V_{bi} - \frac{8.14.10^{-22}.\eta}{c_{ox}.L_{eff}^3}V_{ds} + \gamma.\lambda_s\sqrt{\phi - V_{bs}} + \lambda_n(\phi - V_{bs})$$

$$V_{bi} = V_{T0} - \gamma\sqrt{\phi}$$

$$\lambda_n = \frac{\delta\pi\,\varepsilon_{si}}{2c_{ox}W_{eff}}$$

$$\lambda_s = 1 - \frac{X_j}{L_{eff}}\left(\frac{L_d + W_c}{X_j}\sqrt{1 - \left(\frac{W_p}{X_j + W_p}\right)^2} - \frac{L_d}{X_j}\right)$$

$$W_p = \sqrt{\frac{2\varepsilon_{si}}{qN_{sub}}(\phi - V_{bs})}$$

$$W_c = X_j\left[0.0631353 + 0.8013292\frac{W_p\upsilon}{X_j^{\gamma}} - 0.01110777\left(\frac{W_p}{X_j^{\gamma}}\right)^2\right].$$

Unless γ is assigned a value:

$$\gamma = \frac{\sqrt{2q\varepsilon_{si}N_{sub}}}{c_{ox}}.$$

Unless φ is assigned a value:

$$\phi = 2V_{th}\ln\left(\frac{N_{sub}}{n_i}\right)$$

where n_i is the intrinsic carrier concentration in Silicon

$$L_{eff} = L - 2L_d$$
$$W_{eff} = W - 2W_d.$$

Effective mobility calculations

$$If, V_{\max} \leq 0$$
$$U_{eff} = U_s$$

else

$$U_{eff} = \frac{U_s}{1 + \frac{V_{dsm}}{V_c}}$$

where

$$U_s = \frac{U_0}{1 + \theta(V_{gs} - V_T)}$$
$$V_c = \frac{v_{\max}.L_{eff}}{U_s}.$$

In the saturation region, drain current is modified as follows:

$$I_{ds} = \frac{I_{ds}}{1 - \frac{\Delta L}{L_{eff}}}.$$

If $V_{\max} \leq 0$

$$\Delta L = X_d k \sqrt{V_{ds} - V_{dsat}}$$
$$\Delta L = -\frac{E_p X_d^2}{2}\left[\left(\frac{E_p X_d^2}{2}\right)^2 + \kappa X_d^2 (V_{ds_}V_{dsat})\right]^{1/2}$$
$$E_p = \frac{I_{ds_}at(V_{gs}, V_{dsm}, V_{bs})}{g_{ds}(V_{gs}, V_{dsm}, V_{bs}).L_{eff}}$$
$$X_d = \sqrt{\frac{2\varepsilon_{si}}{q.N_{sub}}}.$$

Acknowledgment

The authors would like to thank TriQuint Semiconductors, Richardson, TX, for allowing access to their TQP13 technology and Prof. V. Popov for engaging in useful discussions.

References

[1] E. Seok, C. Cao, D. Shim, D. J. Arenas, D. B. Tanner, and C. M. Hung, "A 410 GHz CMOS push-push oscillator with an on-chip patch antenna," in *Proc. Int. Solid-State Circuits Conf.*, Feb. 2008, pp. 472–629.

[2] M. Seo, M. Urteaga, J. Hacker, A. Young, Z. Griffith, V. Jain, R. Pierson, P. Rowell, A. Skalare, and A. Peralta, "InP HBT IC technology for terahertz frequencies: Fundamental oscillators up to 0.57 THz," *IEEE J. Solid-State Circuits*, vol. 46, no. 10, pp. 2203–2214, Oct. 2011.

[3] D. Huang, T. R. LaRocca, M. C. F. Chang, L. Samoska, A. Fung, R. L. Campbell, and M. Andrews, "Terahertz CMOS frequency generator using linear superposition technique," *IEEE J. Solid-State Circuits*, vol. 43, no. 12, pp. 2730–2738, Dec. 2008.

[4] M. I. Dyakonov and M. S. Shur, "Plasma wave electronics: Novel terahertz devices using two dimensional electron fluid," *IEEE Trans. Electron Devices*, vol. 43, no. 10, pp. 1640–1645, Oct. 1996.

[5] F. Schuster, D. Coquillat, H. Videlier, M. Sakowicz, F. Teppe, L. Dussopt, B. Giffard, T. Skotnicki, and W. Knap, "Broadband terahertz imaging with highly sensitive silicon CMOS detectors," *Opt. Exp.*, vol. 19, no. 8, pp. 7827–7832, Apr. 2011.

[6] S. Boppel, A. Lisauskas, D. Seliuta, L. Minkevicius, I. Kasalynas, G. Valusis, V. Krozer, and H. G. Roskos, "Silicon CMOS-transistor-based detection up to 4.25 THz," in *Proc. 36th Int. Conf. Infr., Millim. THz Waves*, 2011, pp. 1–2.

[7] T. Watanabe, S. B. Tombet, Y. Tanimoto, Y. Wang, H. Minamide, H. Ito, D. Fateev, V. Popov, D. Coquillat, and W. Knap, "Ultrahigh sensitive plasmonic terahertz detector based on an asymmetric dual-grating gate HEMT structure," in *Proc. Int. Semicond. Device Res. Symp.*, Dec. 2011, pp. 1–2.

[8] M. Dyakonov and M. Shur, "Shallow water analogy for a ballistic field effect transistor: New mechanism of plasma wave generation by dc current," *Phys. Rev. Lett.*, vol. 71, no. 15, pp. 2465–2468, 1993.

[9] A. Dmitriev, A. Furman, and V. Y. Kachorovskii, "Nonlinear theory of the current instability in a ballistic field-effect transistor," *Phys. Rev. B*, vol. 54, no. 19, pp. 14020–14025, 1996.

[10] Y. Deng, R. Kersting, J. Xu, R. Ascazubi, X. C. Zhang, M. S. Shur, R. Gaska, G. S. Simin, M. A. Khan, and V. Ryzhii, "Millimeter wave emission from GaN high electron mobility transistor," *Appl. Phys. Lett.*, vol. 84, no. 1, pp. 70–72, Jan. 2004.

[11] Y. Deng, R. Kersting, J. Xu, R. Ascazubi, X. C. Zhang, M. S. Shur, R. Gaska, G. S. Simin, M. A. Khan, and V. Ryzhii, "Millimeter wave emission from GaN high electron mobility transistor," *Appl. Phys. Lett.*, vol. 84, no. 1, pp. 70–72, Jan. 2004.

[12] D. Zimdars and J. S. White, "Terahertz reflection imaging for package and personnel inspection," *Proc. SPIE*, vol. 5411, pp. 78–83, Sep. 2004.

[13] E. Pickwell and V. Wallace, "Biomedical applications of terahertz technology," *J. Phys. D, Appl. Phys.*, vol. 39, no. 17, p. R301, 2006.

[14] R. Bogue, "Chance discovery of terahertz waveguides by US research group," *Sensors Rev.*, vol. 25, no. 2, pp. 123–124, 2005.

[15] E. R. Mueller and A. J. DeMaria, "Broad bandwidth communication/data links using terahertz sources and Schottky diode modulators/detectors," *Proc. SPIE*, vol. 25, no. 4, pp. 151-1–151-15, Mar. 2005.

[16] *Life Sciences & Chemical Analysis*. (2012) [Online]. Available: http://www.agilent.com

[17] *Cadence Design Systems*. (2012) [Online]. Available: http://www.cadence.com

[18] A. Gutin, V. Kachorovskii, A. Muraviev, and M. Shur, "Plasmonic terahertz detector response at high intensities," *J. Appl. Phys.*, vol. 112, no. 1, pp. 014508-1–014508-5, Jul. 2012.

[19] V. V. Popov, D. V. Fateev, O. V. Polischuk, and M. S. Shur, "Enhanced electromagnetic coupling between terahertz radiation and plasmons in a grating-gate transistor structure on membrane substrate," *Opt. Exp.*, vol. 18, no. 16, pp. 16771-1–16771-6, Aug. 2010.

[20] V. V. Popov, G. M. Tsymbalov, D. V. Fateev, and M. S. Shur, "Cooperative absorption of terahertz radiation by plasmon modes in an array of field-effect transistors with two-dimensional electron channel," *Appl. Phys. Lett.*, vol. 89, no. 12, pp. 123504-1–123504-3, Sep. 2006.

[21] A. Lisauskas, U. Pfeiffer, E. Öjefors, P. H. Bolìvar, D. Glaab, and H. G. Roskos, "Rational design of high-responsivity detectors of terahertzradiation based on distributed self-mixing in silicon field-effect transistors," *J. Appl. Phys.*, vol. 105, no. 11, pp. 114511-1–114511-7, Jun. 2009.

[22] W. Knap, M. Dyakonov, D. Coquillat, F. Teppe, N. Dyakonova, J. Łusakowski, K. Karpierz, M. Sakowicz, G. Valusis, and D. Seliuta, "Field effect transistors for terahertz detection: Physics and first imaging applications," *J. Infr., Millim. THz Waves*, vol. 30, no. 12, pp. 1319–1337, Jul. 2009.

[23] I. Khmyrova and Y. Seijyou, "Analysis of plasma oscillations in high-electron mobility transistorlike structures: Distributed circuit approach," *Appl. Phys. Lett.*, vol. 91, no. 14, pp. 143515-1–143515-3, Oct. 2007.

[24] T. Nishimura, N. Magome, I. Khmyrova, and T. Suemitsu, "Analysis of fringing effect on resonant plasma frequency in plasma wave devices," *Jpn. J. Appl. Phys.*, vol. 48, no. 1, pp. 04C096-1–04C096-4, Apr. 2009.

[25] V. Popov, "Plasmon excitation and plasmonic detection of terahertz radiation in the grating-gate field-effect-transistor structures," *J. Infr., Millim. THz Waves*, vol. 32, no. 10, pp. 1178–1191, Oct. 2011.

[26] W. Knap, V. Kachorovskii, Y. Deng, S. Rumyantsev, J. Q. Lü, R. Gaska, M. Shur, G. Simin, X. Hu, and M. A. Khan, "Nonresonant detection of terahertz radiation in field effect transistors," *J. Appl. Phys.*, vol. 91, no. 11, pp. 9346–9353, Jun. 2002.

[27] W. Stillman, M. S. Shur, D. Veksler, S. Rumyantsev, and F. Guarin, “Device loading effects on nonresonant detection of terahertz radiation by silicon MOSFETs,” *Electron. Lett.*, vol. 43, no. 7, pp. 422–423, Mar. 2007.

[28] M. Sakowicz, M. B. Lifshits, O. A. Klimenko, F. Schuster, D. Coquillat, F. Teppe, and W. Knap, “Terahertz responsivity of field effect transistors versus their static channel conductivity and loading effects,” *J. Appl. Phys.*, vol. 110, no. 5, pp. 054512-1–054512-6, Sep. 2011.

[29] W. Stillman, C. Donais, S. Rumyantsev, M. Shur, D. Veksler, C. Hobbs, C. Smith, G. Bersuker, W. Taylor, and R. Jammy, “Silicon FIN FETs as detectors of terahertz and sub-terahertz radiation,” *Int. J. High Speed Electron. Syst.*, vol. 20, no. 1, pp. 27–42, Mar. 2011

Alexey Gutin received the dual B.S. degree in electrical engineering and computer and systems engineering and the M.S. degree in electrical engineering from the Rensselaer Polytechnic Institute, Troy, NY, in 2007 and 2008, respectively, where he is currently pursuing the Ph.D. degree in electrical engineering.

His current research interests include plasma wave detection of terahertz, high-speed circuit design and modeling, and terahertz imaging sensors.

Trond Ytterdal received the M.Sc. and Ph.D. degrees in electrical engineering from the Norwegian Institute of Technology, Trondheim, Norway, in 1990 and 1995, respectively.

He was a Research Associate with the Department of Electrical Engineering, University of Virginia, Charlottesville, from 1995 to 1996, and was a Research Scientist with the Electrical, Computer and Systems Engineering Department, Rensselaer Polytechnic Institute, Troy, NY, from 1996 to 1997. From 1997 to 2001, he was a Senior ASIC Designer with Nordic Semiconductor, Trondheim. Since 2001, he has been with the Norwegian University of Science and Technology, where he is currently a Professor with the Department of Electronics and Telecommunications. He has authored or co-authored more than 140 scientific papers in international journals and conference proceedings, and has co-authored the books entitled *Semiconductor Device Modeling for VLSI* (Prentice-Hall, 1993), *Introduction to Device Modeling and Circuit Simulation* (Wiley, 1998), and *Device Modeling for Analog and RF CMOS Circuit Design* (Wiley, 2003). He has been a contributor to several other books published internationally and a co-developer of the circuit simulator AIM-Spice. His current research interests include design of analog integrated circuits, behavioral modeling and simulation of mixed-signal systems, modeling of nanoscale transistors, and novel device structures for application in circuit simulators.

Prof. Ytterdal is a member of The Norwegian Academy of Technological Sciences. He was on many Technical Program Committees of the IEEE and other international conferences, including the European Solid-State Circuits Conference, ESSCIRC. He was an Associate Editor of the IEEE TRANSACTIONS ON CIRCUITS AND SYSTEMS II and a Guest Editor for the IEEE JOURNAL OF SOLID-STATE CIRCUITS.

Valentin Kachorovskii was born in Leningrad, Russia, in 1962. He received the Ph.D. degree in semiconductor physics from the Ioffe Physical-Technical Institute, St. Petersburg, Russia, in 1989.

He is currently a Senior Researcher with the Department of the Theory of Electrical and Optical Phenomena in Semiconductors, Ioffe Physical-Technical Institute. He has authored or co-authored over 70 scientific articles published in refereed journals and conference proceedings. His current research interests include transport in disordered systems, spin-dependent phenomena in low-dimensional structures, dynamics of plasma waves, and terahertz electronics.

Andrey Muraviev (native spelling Muravjov) received the Ph.D. degree in physics from the Institute of Applied Physics, Russian Academy of Sciences, Nizhny Novgorod, Russia, in 1992.

He was a Senior Research Scientist with the Institute for Physics of Microstructures, Russian Academy of Sciences, where he was engaged in the development of p-Ge terahertz semiconductor lasers. Since 1997, he has been a Visiting Research Scientist with the University of Central Florida, Orlando, the Rensselaer Polytechnic Institute, Troy, NY, and the University of Buffalo, Buffalo, NY, where he is involved in research on terahertz-related projects. He has authored or co-authored over 70 refereed publications. His current research interests include THz semiconductor lasers and detectors, THz, and mid-IR spectroscopy.

Michael Shur (LF’11) is currently the Roberts Professor and the Acting Director of the Center for Integrated Electronics, Rensselaer Polytechnic Institute, Troy, NY.

Dr. Shur was the recipient of the Tibbetts Award for Technology Commercialization, the St. Petersburg Technical University Honorary Doctorate, the IEEE Kirchmayer Award, the Gold Medal from the Russian Education Ministry, and several Best Paper Awards. He is a Life Member of APS and SPIE, a fellow of OSA, IET, ECS, WIF, MRS, and AAAS, a Life Member of the IEEE MTT, Sigma Xi, and Humboldt Society, and a member of Eta Kappa Nu, Tau Beta Pi, ASEE. He is the Editor-in-Chief of IJHSES, the Vice-President of the IEEE Sensor Council, and a Distinguished Lecturer of the IEEE EDS. He is a Co-founder and the Vice-President of Sensor Electronics Technology, Inc. He is a Foreign Member of the Lithuanian Academy of Sciences.